Applied Catalysis B: Environmental 227 (2018) 349–355

Contents lists available at ScienceDirect

Applied Catalysis B: Environmental

journal homepage: www.elsevier.com/locate/apcatb

Layered cesium copper titanate for photocatalytic hydrogen production

Martin Pilarski[a], Roland Marschall[b,*], Silvia Gross[c], Michael Wark[a]

[a] Institute of Chemistry, Chemical Technology 1, Carl von Ossietzky University Oldenburg, Carl-von-Ossietzky-Str. 9-11, 26129, Oldenburg, Germany
[b] Institute of Physical Chemistry, Justus-Liebig-University Giessen, Heinrich-Buff-Ring 17, 35392, Giessen, Germany
[c] Dipartimento di Scienze Chimiche, Università degli Studi di Padova, and INSTM, UdR Padova, via Marzolo, 1, 35131, Padova, Italy

ARTICLE INFO

Keywords:
Photocatalysis
Hydrogen production
Cu co-catalyst
Localized surface plasmon resonance
Layered materials

ABSTRACT

Layered cesium copper titanate as well as the unmodified cesium titanate $Cs_{0.68}Ti_{1.83}\square_{0.17}O_4$ (□: vacancy) were synthesized by a solution-based approach. The insertion of small amounts of copper into the vacancies of $Cs_{0.68}Ti_{1.83}\square_{0.17}O_4$ led to a significant red shift of the band gap energy from 3.4 eV to 2.9 eV. During photocatalytic H_2 production experiments, a steady increase in the evolution rate was detected, which can be referred to the *in-situ* reduction of incorporated copper ions to metallic Cu. The reduced copper ions leach out of the lattice to the catalyst surface and act as co-catalyst for H_2 formation, considerably exceeding the activity achieved with $Cs_{0.68}Ti_{1.83}\square_{0.17}O_4$ modified with 0.075 wt.-% of Rh as co-catalyst. The use of diffuse reflectance spectroscopy enabled a direct measurement of the copper nanoparticle formation by following their rising plasmon resonance at operating conditions. Characterization by X-ray diffraction (XRD) revealed a significant change in the crystal structure upon photocatalysis.

1. Introduction

The demand for hydrogen as an alternative fuel has grown steadily in recent decades [1]. Photocatalytic active materials for solar hydrogen production represent one promising solution for this increasing request. Nevertheless, most semiconductor materials suffer from large band gaps and fast electron hole recombination, and therefore of low quantum efficiency [2,3]. Two methods are commonly used to decrease the electron hole recombination: i) utilization of methanol [4], ethanol [5] or triethanolamine [6] as sacrificial agents acting as hole scavengers; and ii) deposition of noble metal particles like Rh [7,8], Au [9,10] and Pt [11,12] to establish Schottky contacts for electron trapping. In general, these two methods are applied together to achieve higher activities. However, these techniques are not cost effective because expensive critical metals as well as valuable chemical compounds are used.

Alternatively to critical noble metals, earth-abundant metals or metal oxides like Cu [13–15] and NiO_x [16,17] are deposited as co-catalysts for hydrogen generation. Investigations by Domen et al. [18] in 1998 initiated a revival of copper species as hydrogen evolution co-catalyst. Different publications characterize the active Cu surface component as Cu_2O or Cu/Cu_2O (core/shell) systems primarily investigated on TiO_2 [13,19,20]. The presence of Cu(I) species is verified by X-ray photoelectron spectroscopy (XPS) measurements [13,19]. Nevertheless, most of the commonly used characterization methods like XPS, X-ray diffraction (XRD), absorption spectroscopy, chemisorption, physisorption, transmission and scanning electron microscopy (TEM, SEM) provide only characterization data of the catalyst or co-catalyst status *ex-situ* before and after the photocatalytic process. In contrast, localized surface plasmon resonance (LSPR) spectroscopy enables an *in-situ* observation of the formation of the plasmon active co-catalyst during photocatalytic H_2 production and gives first insights of the actually operating co-catalyst [21].

The layered cesium titanate $Cs_{0.68}Ti_{1.83}\square_{0.17}O_4$ (□: vacancy) consists of a lepidocrocite γ-FeOOH-type layered structure [22] and represents a good starting material for further modifications with regard to the incorporation of cations [23–25] and anions [26] for band gap reduction, due to its open layered structure and the theoretical amount of 0.17 equivalents of vacancies distributed in the titanium oxide sheets, which are spatially separated by cesium cations. This material enables a simple insertion of, for example, Mg, Fe, Co, Ni, Cu or Zn ions into the vacancies of the titanate sheets. Up to now, the cation modification and the synthesis of the base material have been mainly performed by solid state reaction (SSR) [23,24,27]. However, SSR requires high calcination temperatures [27] and long calcination times [28], resulting in a highly crystalline material but characterized by large particle sizes. A main drawback of the SSR for cation doping can be an inhomogeneous distribution of the inserted metal cation through the catalyst material because of the slow diffusion rate of ions in solids during the calcination period. Already in 2001 Sumida et al. presented

* Corresponding author.
E-mail address: roland.marschall@phys.chemie.uni-giessen.de (R. Marschall).

https://doi.org/10.1016/j.apcatb.2018.01.039
Received 17 November 2017; Received in revised form 15 January 2018; Accepted 16 January 2018

an alternative synthesis of $Cs_{0.68}Ti_{1.83}\square_{0.17}O_4$ by employing the polymerized complex (PC) method applying citrate ions and ethylene glycol as complexing agent [28]. Cation modification of materials prepared *via* solution-based routes can minimize the inhomogeneity issue because of the improved dispersion of the metal ions. Additionally, a solution-based method like the PC-route allows the synthesis of mixed metal oxides at lower calcination temperatures in shorter reaction times, as shown in this work.

In this paper, the properties of layered cesium copper titanate for photocatalytic H_2 generation are presented and discussed. The *in-situ* formation of metallic Cu as co-catalyst on the photocatalyst surface is followed by Cu LSPR, and an explicit effect on the long-term hydrogen evolution is observed. Structural changes after H_2 production are investigated in detail, leading to new insights into the tested photocatalyst.

2. Experimental

2.1. Catalyst preparation

Cesium copper titanates were synthesized by a complex-based process similar to the PC method [29–31]. The photocatalysts were synthesized by an aqueous citrate-based method [30–32]. The used quantities of the metal compounds correspond to the stoichiometric composition of $Cs_{0.68}Ti_{1.83}O_4$. Basing on this formula relative to cesium a 3 at.-% excess of Ti was used in the synthesis in order to obtain complete phase purity. In the synthesis of Cu containing cesium titanates, Copper ions were added to the synthesis batches in Cu: Cs atomic ratios of 1:7 and 1:14, respectively.These amounts were chosen in order to tune the amount of structural vacancies. Citric acid monohydrate and ethylene diamine tetra acetic acid (EDTA) were utilized as complexing reagents. 8.23 g (28.16 mmol) EDTA and 8.51 g (40.49 mmol) citric acid were dissolved in a mixture of 580 mL deionized water and 18.5 mL of 33% ammonium hydroxide solution. After adjusting the pH value at pH = 5 with 65% nitric acid (HNO_3), 1.36 g cesium nitrate ($CsNO_3$ Sigma Aldrich 99.99%) and 0.12 g or 0.24 g copper nitrate trihydrate ($Cu(NO_3)_2{\cdot}3H_2O$, Sigma-Aldrich, 99.99%), each dissolved in 25 mL deionized water, were inserted into the complexing reagent solution. Pre-diluted 6.53 mL titanium(IV)-*n*-butoxide (Sigma-Aldrich, > 97%) in 240 mL absolute ethanol were added to the mixture. After evaporation to approximately 25 mL at 373 K, the produced gel was transferred to a ceramic bowl and heated at 723 K. The so obtained powder precursor was calcined in air at 873 K for 10 h.

2.2. Characterization

XRD measurements were carried out to characterize the phase composition of the calcined samples. Diffraction patterns were recorded in reflection geometry with a PANalytical Empyrean Theta-Theta diffractometer equipped with a copper tube (K_α = 0.154 nm), 0.25° divergent slit, 0.5° anti scatter slit (incident beam), 7.5 mm high anti scatter slit (diffracted beam), incident and diffracted beam 0.04 rad soller slits, and position sensitive PIXcel-1d detector. The Cu-K_β emission line is suppressed by a nickel filter. For qualitative phase analysis the specimen were scanned in the 5–50° 2θ range with a step width of 0.0131° and 200 s collection time per step at an ambient temperature of 300 K.

UV–vis diffuse reflectance spectra were measured on a Varian Cary 4000 UV–vis spectrophotometer equipped with an integrating sphere. Spectra were collected in the range of 200–800 nm. MgO was used as a white standard material. Band gap energies were determined by constructing Tauc plots for an indirect semiconductor from the calculated Kubelka-Munk functions of the respective diffuse reflectance spectra. The band gap energies were estimated by extrapolation of the absorption edge to the energy axis of the Tauc plot. Investigation of the LSPR was performed on the above mentioned UV–vis spectrophotometer under the same conditions. For the LSPR measurement 3 mL of the catalyst suspension were taken out of the reactor and transferred into a full quartz cuvette. The cuvette was placed in front of the integrating sphere. The MgO reference was placed on the back side of the cuvette to ensure all scattered light being reflected back to the detector.

The surface compositions of the prepared compounds, the chemical environment, oxidation states of the species of interest were investigated by XPS. Spectra were run on a Perkin-Elmer Φ 5600ci spectrometer using standard Mg radiation (1253.6 eV) working at 250 W, to avoid signal overlaps occurring by using the Al source. The working pressure was $< 5*10^{-8}$ Pa. The spectrometer was calibrated by assuming the binding energy of the $Au4f_{7/2}$ line at 83.9 eV with respect to the Fermi level. The standard deviation for the binding energy values was 0.15 eV. The reported binding energies were corrected for the charging effects by assigning the C1s line to a binding energy of 284.6 eV. Survey scans (187.85 pass energy, 0.4 eV/step, 25 ms per step) were obtained in the 0–1200 eV range. Detailed scans (29.35 eV pass energy, 0.1 eV/step, 100–150 ms per step) were recorded for the C1s, O1s, N1s, Ti2p, Ti_{LMM}, Cu2p, Cu_{LMM}, Cs3d regions. The atomic composition was evaluated, after a Shirley type background subtraction, using sensitivity factors supplied by Perkin Elmer. The assignment of the signals was carried out by using values reported in the reference handbook, in the NIST XPS database.

HR-TEM measurements were performed on a JEOL JEM2100F transmission electron microscope. Au sample grids with 200 meshes were used for HR-TEM measurements.

X-ray fluorescence spectroscopy (XFS) measurements for element analysis were performed on a Philips PW 2400 wavelength dispersive X-ray fluorescence spectrometer.

All energy dispersive X-ray spectroscopic measurements were performed on a Helios NanoLab 600i scanning electron microscope from FEI.

2.3. Photocatalytic hydrogen production

Photocatalytic H_2 production was performed in a double-walled semi-batch glass reactor. The reactor was cooled down to 283 K by a cryostat (Lauda) to prevent any thermal influence on the tested photocatalyst. The reaction medium consists of 550 mL water, 50 mL of methanol as a sacrificial agent, and 500 mg of the investigated photocatalyst. Before irradiation, the reactor was degassed in an Argon flow of 200 NmL. The catalyst suspension was irradiated with UV–vis light by a 500 W Hg mid pressure immersion lamp (Peschl Ultraviolet) without optic filters. During irradiation a carrier gas flow of argon (Ar 6.0) was set to 50 NmL/min by a mass flow controller for the transport of the produced gases to the detection unit. The evolved H_2 was detected by a thermal conductivity detector in a multi gas analyzer from Emerson.

3. Results and discussion

During incorporation of additional elements into the crystal structure of a metal oxide, the overall charge neutrality of the host material has to be kept. For the compensation of the Cu substitution, in principle a decrease in the titanium and cesium content or an increase in the vacancy amount may occur. X-ray fluorescence analysis for element determination was performed in order to clarify the accurate stoichiometric composition of the cesium copper titanates. According to the stoichiometry of $Cs_{0.63}Ti_{1.82}Cu_{0.05}O_4$ and $Cs_{0.64}Ti_{1.79}Cu_{0.1}O_4$ calculated from X-ray fluorescence measurements (table S1, S2 Supporting Information SI) for the obtained cesium copper titanates, the lowered cesium and titanium contents in comparison to $Cs_{0.68}Ti_{1.83}\square_{0.17}O_4$ lead to the conclusion of a dual A and B-site occupation by Cu ions or rather to a dual incorporation of Cu^+ ions into the titanate sheets and the interlayers.

Fig. 1 shows the XRD patterns and the Tauc plots of

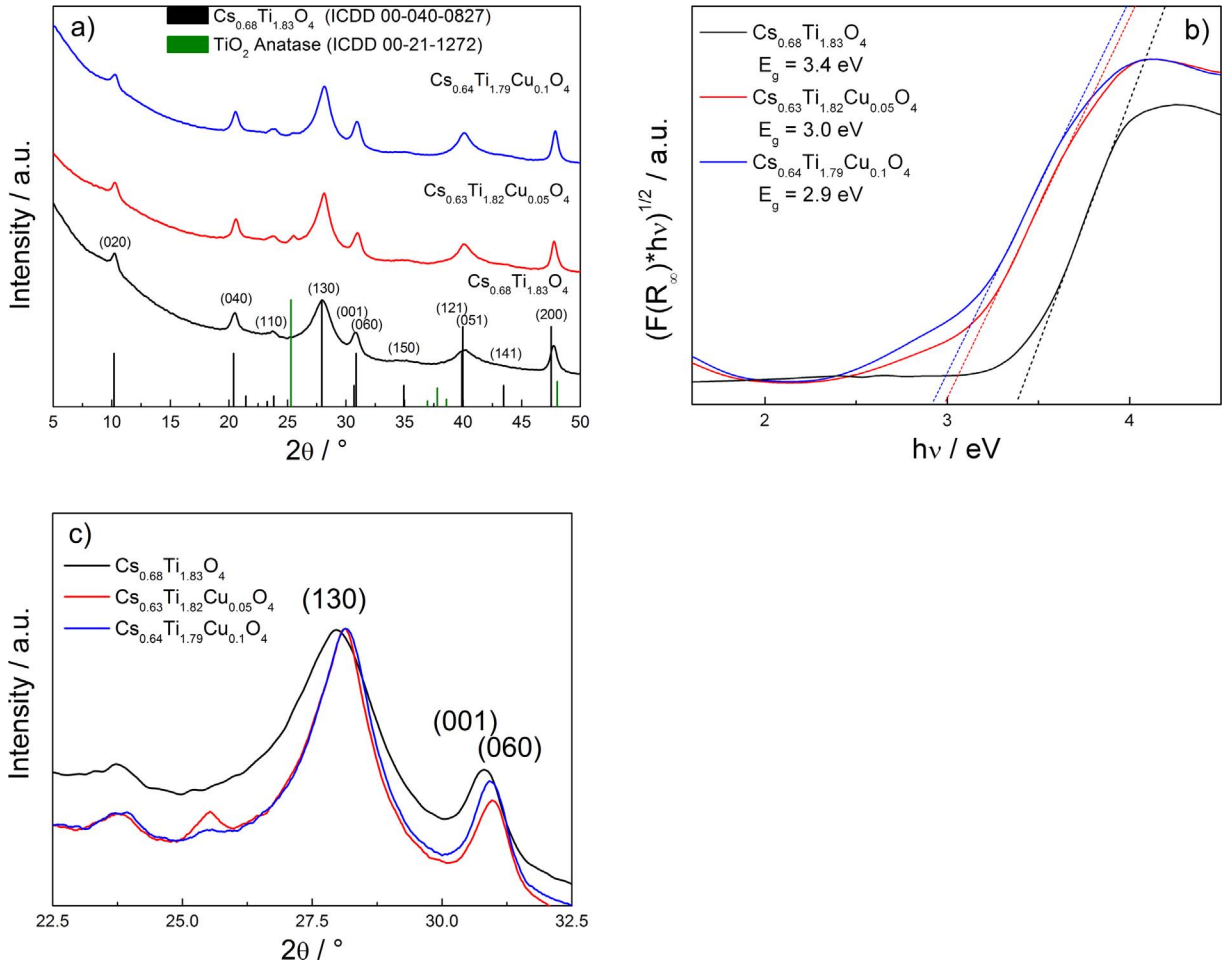

Fig. 1. a) XRD patterns, b) Tauc plots of $Cs_{0.68}Ti_{1.83}\square_{0.17}O_4$, $Cs_{0.63}Ti_{1.82}Cu_{0.05}O_4$ and $Cs_{0.64}Ti_{1.79}Cu_{0.1}O_4$ and c) magnified section of the range 22.5–32.5° 2θ in the XRD patterns.

$Cs_{0.68}Ti_{1.83}\square_{0.17}O_4$, $Cs_{0.63}Ti_{1.82}Cu_{0.05}O_4$ and $Cs_{0.64}Ti_{1.79}Cu_{0.1}O_4$ prepared by solution-based synthesis, respectively.

This approach enables the synthesis of layered cesium titanates at lower temperatures and shorter calcination times compared to the classic SSR [33]. To prevent the formation of the undesired cesium titanate compounds $Cs_2Ti_4O_9$ [34] (main impurity) and $Cs_{1.1}Ti_8O_{16}$ [35] a 3 at.-% excess of the Ti-precursor was found to be necessary in the synthesis of $Cs_{0.68}Ti_{1.83}\square_{0.17}O_4$. However, the thus formed materials contain some traces of TiO_2. The TiO_2 impurity was identified as anatase by the most intense reflection (011) at 25.5° 2θ. No CuO or Cu_2O crystalline phases could be observed in the XRD patterns indicating a homogenous distribution of Cu ions. However, the insertion of Cu ions leads to shifts of some reflections, *e.g.* the intense reflection (130) shifts from 27.9° to 28.1° 2θ, as shown in Fig. 1c, indicating a contraction of the distance between the crystallographic planes in the layered material. The reflection at around 31° 2θ shifts, in detail from 30.81° for $Cs_{0.68}Ti_{1.83}\square_{0.17}O_4$ to 30.98° for $Cs_{0.63}Ti_{1.82}Cu_{0.05}O_4$ and to 30.93° 2θ for $Cs_{0.64}Ti_{1.79}Cu_{0.1}O_4$. It does not correspond to the observed signal shift of the most intensive (130) reflection at around 28° 2θ. However, the reflection at around 31° 2θ is not appropriate to quantify the influence of the inserted Cu ions to the lattice contraction of the produced materials because it results as a combination of the overlapping (010) and (060) reflections, as shown in Fig. 1a. The reflections of the (010) and (060) lattice plane cannot be distinguished due to the low crystallinity of the used materials. The increased background induced by the most intensive (130) reflection additionally influences the neighboring reflex position, abd with that also the combined (010) and (060) reflections. In further detail, a similar situation can be also observed for the reflection at around 40° 2θ. The intensity and position of this reflection is influenced by the combination of the (121) and (051) reflections, and is therefore also not appropriate to quantify the effect of inserted Cu ions on the crystal lattice. Furthermore, the (200) reflection at around 40° 2θ is influenced by the anatase impurity and is for this reason not appropriate as well. Reflections in the lower 2θ range below 25° are influenced by the high background, which arises from the utilized XRD setup. Due to this circumstance, only the most intensive (130) reflection was chosen for quantification because of the absence of influence by other lattice planes and a minimum of background shift.

The insertion of small amounts of Cu also results in changes of the band gap energy, reducing the initial band gap of 3.4 eV for $Cs_{0.68}Ti_{1.83}\square_{0.17}O_4$ down to 3.0 eV ($Cs_{0.63}Ti_{1.82}Cu_{0.05}O_4$) or 2.9 eV ($Cs_{0.64}Ti_{1.79}Cu_{0.1}O_4$), respectively. The extrapolation of the absorption edges of the Cu modified layered cesium titanates is not straightforward. The curve shape suggests a second absorption edge beginning around 3.2 eV, tailing into the visible light region. The signal shape can be referred to a highly dispersed Cu oxide species Cu_xO (x = 1, 2) in the titanate sheets [36], or single Cu-O transitions due to the incorporation of Cu ions. Despite of the homogenously distributed Cu ions, the Cu-O transition has a significant influence on the absorption property of $Cs_{0.63}Ti_{1.82}Cu_{0.05}O_4$ and $Cs_{0.64}Ti_{1.79}Cu_{0.1}O_4$. This is, to the best of our knowledge, the first example of band gap reduction of $Cs_{0.68}Ti_{1.83}\square_{0.17}O_4$ by Cu cations to achieve visible light absorption. Cu^{2+} species in an octahedral coordination may form additional energy states in the band structure of the presented cesium copper titanates. The octahedral splitting of the Cu 3d orbitals additionally contributes to the band gap lowering. In summary, the lowered band gap energies of $Cs_{0.63}Ti_{1.82}Cu_{0.05}O_4$ and $Cs_{0.64}Ti_{1.79}Cu_{0.1}O_4$ arise from two effects, first the hybridization of Ti 3d and Cu 3d orbitals from incorporated Cu ions

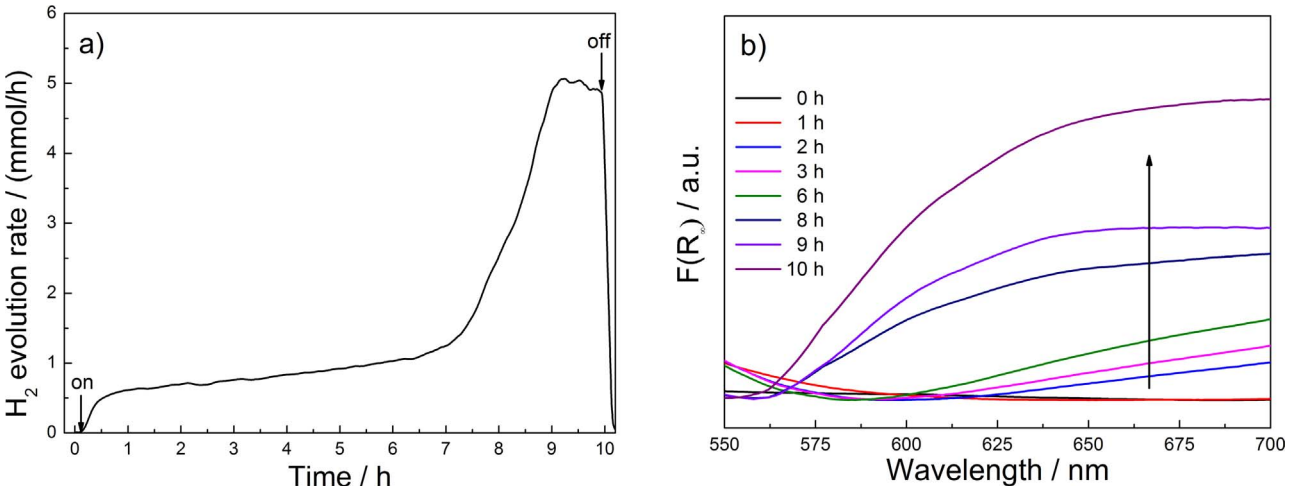

Fig. 2. a) Photocatalytic H_2 production in methanol/water mixture with $Cs_{0.64}Ti_{1.79}Cu_{0.1}O_4$, b) corresponding LSPR spectra, recorded during H_2 production.

in the titanate sheets, and from octahedral splitting of the Cu 3d-orbitals in an octahedral coordination in the titanates interlayer.

3.1. Photocatalytic H_2 production and LSPR

To investigate the effect of the Cu incorporation on the photocatalytic activity, samples characterized by two different amounts of copper, marked as $Cu_{0.05}$ (1.285 wt.-%) and $Cu_{0.1}$ (2.57 wt.-%) were used. Primary, only the higher loaded material is discussed in this paper, but the same phenomena were found to occur also in the material with lower Cu content.

The non-modified semiconductor $Cs_{0.68}Ti_{1.83}\square_{0.17}O_4$ is able to generate hydrogen from water/methanol mixtures without any co-catalyst (Fig. S1 SI). After stepwise photodeposition of very low amounts of Rhodium (Rh) as co-catalyst, a maximum hydrogen evolution steady state rate of 3.1 mmol/h H_2 can be reached with 0.075 wt.-% Rh.

Fig. 2a shows the H_2 evolution rate of $Cs_{0.64}Ti_{1.79}Cu_{0.1}O_4$, and in Fig. 2b the simultaneously recorded LSPR spectra are given. During 7 h of irradiation, a steadily increasing H_2 evolution rate was observed. After 7 h an exponential increase took place up to a rate of 5.1 mmol/h. Afterwards, during 10 h of constant irradiation, the H_2 evolution rate decreased to 4.8 mmol/h indicating slow deactivation.

The LSPR signal shapes strongly depend on the particle size, particle shape and the chemical environment which all influence the dielectric constant of the metal particles [21,37,38]. Fig. 2b shows selected LSPR spectra to visualize the fate of Cu cations being reduced during photocatalytic H_2 production. A blank measurement (0 h) shows no LSPR features corresponding to metallic Cu. In the initial phase of irradiation, $Cs_{0.64}Ti_{1.79}Cu_{0.1}O_4$ and $Cs_{0.68}Ti_{1.83}\square_{0.17}O_4$ show a comparable activity of 0.6 mmol/h (Fig. S1 SI), and the corresponding LSPR spectra do not differ. After 2 h of irradiation the LSPR transition signal is constantly increasing; however the signals are broad and asymmetric, thus indicating a broad particle size and shape distribution. An increase in signal intensity at 600 nm after 8 h corresponds to the exponential increase of the H_2 evolution rate, marking a strong activation due to the formation of a critical amount of metallic Cu, which can act as a co-catalyst. This long activation period can be explained by a slow diffusion of the reduced Cu ions from the bulk of $Cs_{0.64}Ti_{1.79}Cu_{0.1}O_4$ network to the outer surface. Thus, the photocatalytic H_2 production and the Cu cation reduction are parallel reactions taking place at the same time. $Cs_{0.64}Ti_{1.79}Cu_{0.1}O_4$ reaches a H_2 evolution rate of about 5 mmol/h, exceeding that of $Cs_{0.68}Ti_{1.83}\square_{0.17}O_4$ considerably.

During irradiation the color of the catalyst suspension turns from faint yellow to black. The final color indicates a high dispersion of the metallic Cu co-catalyst on the photocatalyst surface. After exposure to air the catalyst suspension decolorized to pale green, indicating an oxidation of exposed Cu nanoparticles from Cu(0) to Cu(II). A photometric analysis of the reaction solution confirmed that no copper was released to the solution, Cu is still bound on the host material and is not washed out during the photocatalytic process.

Interestingly, in further photocatalytic runs with recovered and reused $Cs_{0.64}Ti_{1.79}Cu_{0.1-x}O_4$, the oxidized Cu particles, formed during catalyst recovery in air, were easily reduced, rebuilding the Cu co-catalyst (Fig. S2a SI). The co-catalyst formation immediately starts in the beginning of the irradiation period. The corresponding LSPR spectra (Fig. S2b SI), showing no absorption at 0 h, reveal that no metallic Cu is available on the photocatalyst surface before irradiation.

However, the reused photocatalyst suffers from a decreased activity which is reflected in a lower initial H_2 evolution rate of 3.8 mmol/h. Probably, some agglomeration of the initially *in-situ* formed Cu nanoparticles occurs during oxidation and reduction.

A stabilization of the inserted Cu ions in the crystal lattice can be achieved by a further calcination step at 800 °C for 10 h. But this temperature treatment leads to a decreased photocatalytic activity in H_2 production of only 0.4 mmol/h, because no metallic Cu nanoparticles, which can act as co-catalyst, could form (Fig. S3 SI).

$Cs_{0.63}Ti_{1.82}Cu_{0.05}O_4$ shows a similar behaviour in its photocatalytic activity and in the respective LSPR spectra. However, $Cs_{0.63}Ti_{1.82}Cu_{0.05}O_4$ suffers from an extended activation time and lower activity in H_2 production (Fig. S4 SI). The extended activation time can be explained by a lower probability of Cu ion reduction due to the lower amount of Cu ions, and a preferred H_2 production. The decreased H_2 evolution rate can also be referred to the lower amount of active co-catalyst.

The presented hydrogen evolution rates and the respective intensities of copper SPR absorbance from $Cs_{0.63}Ti_{1.82}Cu_{0.05}O_4$ and $Cs_{0.64}Ti_{1.79}Cu_{0.1}O_4$ indicate a direct correlation between them. Another sample with more or less copper incorporation might further support this conclusion. However, in the used synthesis approach, higher copper contents lead to the formation of undesired $Cs_2Ti_4O_9$. Lower copper contents show no effect on the band gap energy and no increased photocatalytic activities.

$Cs_{0.64}Ti_{1.79}Cu_{0.1}O_4$ and reused $Cs_{0.64}Ti_{1.79}Cu_{0.1-x}O_4$ show no activity under visible light irradiation. Therefore, a contribution of Cu SPR absorbance to the photocatalytic activity or rather the excitation of Cu plasmons, which are transported to the conduction band of the host photocatalyst, can be excluded.

The results reveal that differently sized Cu particles are formed by the citrate route, which can be observed by a broad LSPR signal, and they act as suitable co-catalyst species on appropriate reaction sites. The direct occupation of reaction sites during photoinduced reduction manifests in a high H_2 evolution rate.

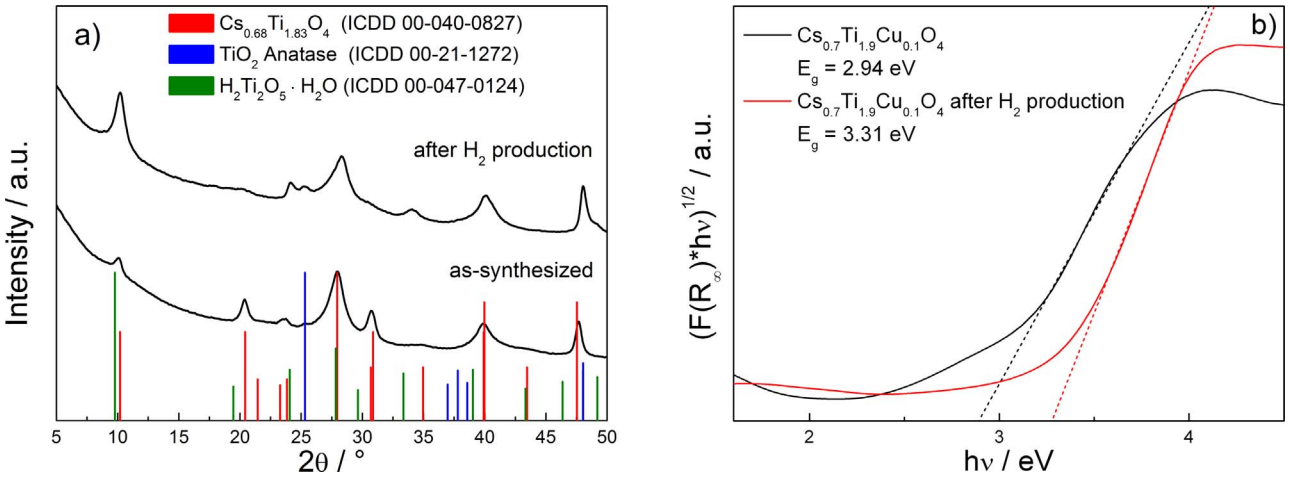

Fig. 3. a) XRD patterns and b) Tauc plots of $Cs_{0.64}Ti_{1.79}Cu_{0.1}O_4$ before and after photocatalytic H_2 production.

The color change after photocatalytic H_2 production and the observed deactivation indicate changes in crystal structure and optical properties of all tested catalysts, which are confirmed by post-photocatalytic XRD analysis and Tauc plots (Fig. 3).

XRD analysis of the used photocatalyst $Cs_{0.64}Ti_{1.79}Cu_{0.1-x}O_4$ showed the existence of a cesium-depleted material displaying the chemical formula $H_2Ti_2O_5{\cdot}H_2O$ (Fig. 3a). Two lattice planes from $Cs_{0.64}Ti_{1.79}Cu_{0.1}O_4$ at 21.4° and 30.8° 2θ are no longer detected while the reflection at 10.4° 2θ rises in intensity after H_2 production.

Such cesium cation exchange by protons is known for $Cs_{0.68}Ti_{1.83}\square_{0.17}O_4$. It was observed in acidic media like 1 M HCl after 2–3 days of constant stirring of SSR material [21,39] or for sol-gel derived materials calcined at 800 °C [40]. The XPS measurements, which will be discussed in Section 3.2 confirm the cation exchange.

The removal of Cu ions from the bulk during photocatalytic H_2 production is effectively observed by UV–vis spectroscopy. Band gaps calculated from Tauc plots show an increase to 3.31 eV for $Cs_{0.64}Ti_{1.79}Cu_{0.1-x}O_4$ (Fig. 3b). This fact reveals that in case of $Cs_{0.64}Ti_{1.79}Cu_{0.1-x}O_4$ nearly all of the incorporated Cu ions are reduced or rather removed from the bulk and attached on the photocatalyst surface. It might be expected that the *in-situ* formation of $H_2Ti_2O_5{\cdot}H_2O$ promotes the leaching effect of the reduced Cu ions.

3.2. Transmission electron microscopy and X-ray photoelectron spectroscopy

Generally, all TEM images of the prepared cesium copper titanates show the same irregular and inhomogeneous shape of theirparticles, as seen in Fig. 4a. The particle form is referred to the citrate route for the synthesis of $Cs_{0.64}Ti_{1.79}Cu_{0.1}O_4$ and $Cs_{0.63}Ti_{1.82}Cu_{0.05}O_4$ producing flake-like primary particles with ragged edges. These primary particles agglomerate to bigger aggregates of different size. EDX-based elemental analysis of the as-synthesized $Cs_{0.64}Ti_{1.79}Cu_{0.1}O_4$ particles shows Cu being homogeneously distributed throughout the material (Fig. S6/Table S3, Fig. S7/Table S4, Fig. S8/Table S5 SI).

Estimation of an average particles size of the Cu particles by TEM is not possible because of their strong agglomeration. However, *in-situ* recorded LSPR spectra indicate a variety of different particles sizes and shapes, which manifests in a broad signal (Fig. 2b). Such Cu particles could not be found in the as-synthesized $Cs_{0.64}Ti_{1.79}Cu_{0.1}O_4$; consequently the Cu particles observed in the recovered sample arise from the photocatalytic process. High resolution imaging enables the visualization of the layered structure of this material class (Fig. 4b) and also proofs that the sheet-like structure remains intact after H_2 production.

For a better understanding of the chemical evolution of the photocatalyst surface upon photocatalytic activity, XPS measurements of the as-synthesized and of the recovered $Cs_{0.64}Ti_{1.79}Cu_{0.1}O_4$ samples were performed. The position of the Ti2p and Cs $3d_{5/2}$ regions display, after correction for charging effects based upon the position of the C1s signal relative to adventitious carbon at 284.6 eV, the typical binding energies of Ti(IV) (Fig. S8 SI) and Cs(I) in oxidic environment, whereas the presence of Ti(III) (~456.8 eV) and metallic cesium (~726 eV) could be definitely excluded. All measured binding energies of as-synthesized and recovered photocatalysts are in the binding energy range of Ti(IV) and Cs(I) [41,42]. The observed shifts are, though small, towards higher binding energy, which is indicative either of an increase in

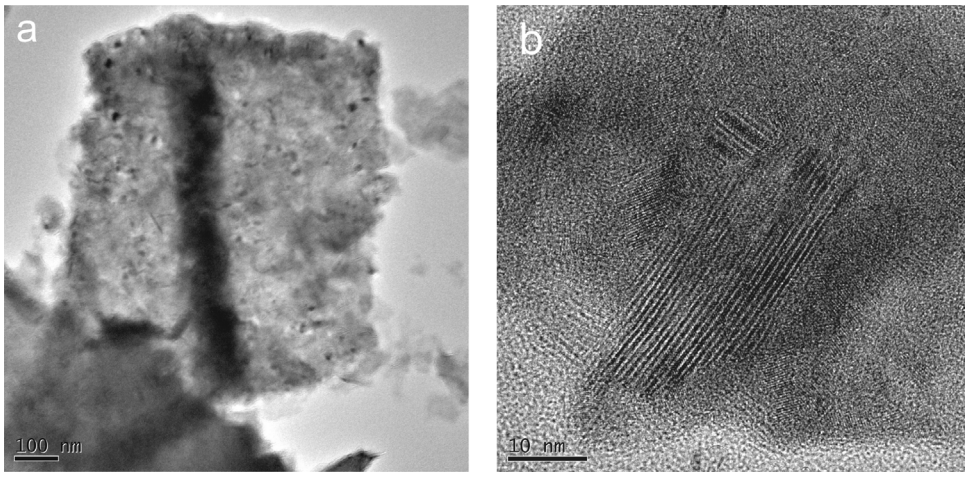

Fig. 4. a) TEM and b) HR-TEM image of $Cs_{0.64}Ti_{1.79}Cu_{0.1}O_4$ after photocatalytic H_2 production.

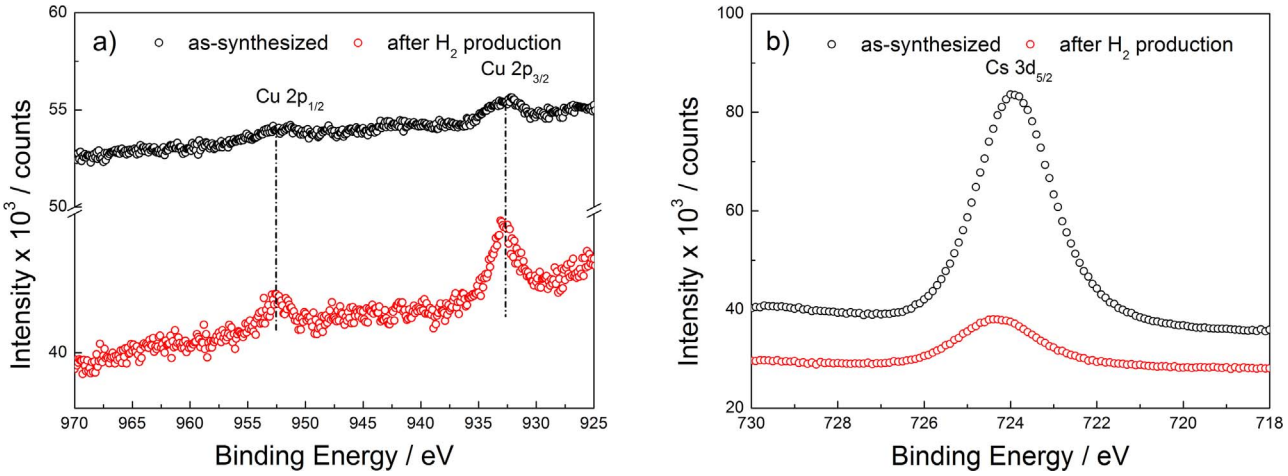

Fig. 5. XP spectra of a) Cu $2p_{1/2}$ and Cu $2p_{3/2}$ components of Cu2p and b) Cs $3d_{5/2}$ signal (values corrected for charging effects) of as-synthesized and recovered $Cs_{0.64}Ti_{1.79}Cu_{0.1}O_4$.

oxidation state (which could however be ruled out in this case, since Ti (IV) cannot be oxidized) or of a more electronegative chemical environment, possibly related to the changes occurred upon the photocatalytic reaction.

The corrected binding energy of the Cu $2p_{3/2}$ signal is in the range of 932.2–932.8 eV (Fig. 5a), being lower than values expected for Cu(II) (> 933.4 eV) [42,43]. However, to get stronger evidence about the oxidation state of copper, the kinetic energy of the Cu_{LMM} Auger transition was used to calculate the respective Auger parameter. The Cu Auger parameter of $Cs_{0.64}Ti_{1.79}Cu_{0.1}O_4$ shows different values before (1849.0 eV) and after (1848.1 eV) photocatalysis, both values being also quite different from the expected metallic Cu (1851.0–1851.3 eV) [42,43]. Instead, these values seem to hint at the presence of Cu(I) (1848.6–1849.6 eV), since Cu(II) in CuO is as well characterized by a higher Auger parameter (~1851 eV) [41,42]. It seems that Cu(I) oxide species are present in contact with air, which can be reduced to metallic Cu during photocatalytic H_2 production (Fig. 2).

The formation of a Cu(I) species from a Cu(II) precursor might be questionable since Cu_2O can be formed by the thermal reduction of CuO only at temperatures above 800 °C. However, certain organic ligands are capable to reduce Cu(II) to Cu(I) [44]. Therefore one possible explanation is the reduction by the used complexing agents EDTA and citric acid.

The detected decrease in the atomic percentage of copper upon photocatalysis can be attributed to leaching phenomena occurring in the materials.

Furthermore, from the intensities of the Cs $3d_{5/2}$ signals before and after photocatalytic H_2 production (Fig. 5b) a decrease from 4.6 at.-% (before) to 1.0 at.-% (after photocatalysis) is calculated by quantitative analysis. This change in cesium content can be ascribed to a leaching of the ions upon photocatalysis, or it might hint at a change in crystal structure after H_2 production by the exchange of cesium ions by protons, as pointed out above. Concerning the slight shift from 724.0 eV to 724.3 eV of the binding energy values of the Cs$3d_{5/2}$ region upon H_2 production, this can be tentatively ascribed to a slightly less electronegative charge-withdrawing environment around the cesium ions. It has already been reported that the physical basis of the short-range core-level chemical shift of Cs $3d_{5/2}$ binding energy is the difference in electronic charge around the Cs ions [45]. In combination with XRD measurements the formation of $H_2Ti_2O_5{\cdot}H_2O$ and $H_{0.64}Ti_{1.79}Cu_{0.1}O_4$ during the photocatalytic process could be verified. Since cesium cations are still present after the photocatalytic process, a coexistence of all the different materials must be expected.

4. Conclusions

The paper demonstrates that Cu^{2+} ions incorporated into the layered cesium titanate $Cs_{0.68}Ti_{1.83}\square_{0.17}O_4$ with lepidocrocite structure by the citrate route act as a pre-inserted precursor allowing an easy *in-situ* formation of an active, cheap and abundant co-catalyst for photocatalytic H_2 production.

During photocatalysis, $Cs_{0.64}Ti_{1.79}Cu_{0.1}O_4$ is subjected to a change in crystal structure due to the exchange of cesium ions by protons. Furthermore, the band gap energy changes since the band gap lowering effect by the Cu^{2+} is lost, due to their extraction from the lattice and reduction to metallic copper during photocatalytic H_2 production.

LSPR spectroscopy was used to investigate the *in-situ* formation of metallic Cu co-catalyst nanoparticles. $Cs_{0.64}Ti_{1.79}Cu_{0.1}O_4$ prepared by citrate route provides broad signals in the LSPR spectra during photocatalysis due to broad particle size and shape distribution of the formed Cu nanoparticles as confirmed by TEM images.

Cu co-catalyst nanoparticles are very effective, leading to an increase of the H_2 evolution rate by a factor of 10, since the Cu^{2+} ions from the lattice are directly reduced at the sites where H_2 is originally generated, leading to very effective Schottky contacts.

Further work is necessary with respect to the stabilization of these Cu co-catalyst particles after contact with air, and to investigate the influence of the Cu co-catalyst formation on educt adsorption.

Acknowledgements

R.M. gratefully acknowledges funding in the Emmy-Noether program (MA 5392/3-1) of the German Research Foundation DFG. M.W. acknowledges financial support by the DFG within the priority program SPP 1613 (MW 1116/28-1).

Appendix A. Supplementary data

Supplementary data associated with this article can be found, in the online version, at https://doi.org/10.1016/j.apcatb.2018.01.039.

References

[1] R.M. Navarro Yerga, M.C. Alvarez Galvan, F. del Valle, J.A. Villoria de la Mano, J.L.G. Fierro, Water splitting on semiconductor catalysts under visible-light irradiation, ChemSusChem 2 (2009) 471–485.
[2] F.E. Osterloh, Inorganic materials as catalysts for photochemical splitting of water, Chem. Mater. 20 (2008) 35–54.
[3] A. Kudo, Y. Miseki, Heterogeneous photocatalyst materials for water splitting, Chem. Soc. Rev. 38 (2009) 253–278.
[4] M. Shen, M.A. Henderson, Identification of the active species in photochemical hole scavenging reactions of methanol on TiO_2, J. Phys. Chem. Lett. 2 (2001)

2707–2710.
[5] G.R. Bamwenda, S. Tsubota, T. Nakamura, M. Haruta, Photoassisted hydrogen production from a water-ethanol solution: a comparison of activities of Au/TiO_2 and Pt/TiO_2, J. Photochem. Photobiol. A: Chem. 89 (1995) 177–189.
[6] S. Ikeda, C. Abe, T. Torimoto, B. Ohtani, Photochemical hydrogen evolution from aqueous triethanolamine solutions sensitized by binaphthol-modified titanium(IV) oxide under visible-light irradiation, J. Photochem. Photobiol. A: Chem. 160 (2003) 61–67.
[7] K. Maeda, K. Teramura, D. Lu, N. Saito, Y. Inoue, K. Domen, Noble-metal/Cr_2O_3 Core/Shell nanoparticles as a cocatalyst for photocatalytic overall water splitting, Angew. Chem. Int. Ed. 45 (2006) 7806–7809.
[8] K. Yamaguti, S. Sato, Photolysis of water over metallized powdered titanium dioxide, J. Chem. Soc. Faraday Trans. 81 (1985) 1237–1246.
[9] R. Kydd, K. Chiang, J. Scott, R. Amal, Low energy photosynthesis of gold-titania catalysts, Photochem. Photobiol. Sci. 6 (2007) 829–832.
[10] J. Chen, J.C.S. Wu, D.P. Tsai, Plasmonic Photocatalyst for H_2 evolution in photocatalytic water splitting, J. Phys. Chem. C 115 (2011) 210–216.
[11] P. Panagiotopoulou, E.E. Karamerou, D.I. Tsai, Kinetics and mechanism of glycerol photo-oxidation and photo-reforming reactions in aqueous TiO_2 and Pt/TiO_2 suspensions, Catal. Today 209 (2013) 91–98.
[12] S. Sato, J.M. White, Photodecomposition of water over Pt/TiO_2 catalysts, Chem. Phys. Lett. 72 (1980) 83–86.
[13] W.J. Foo, C. Zhang, G.W. Ho, Non-noble metal Cu-loaded TiO_2 for enhanced photocatalytic H_2 production, Nanoscale 5 (2013) 759–764.
[14] J. Yu, Y. Hai, M. Jaroniec, Photocatalytic hydrogen production over CuO-modified titania, J. Colloid Interface Sci. 357 (2011) 223–228.
[15] V. Gombac, L. Sordelli, T. Montini, J.J. Delgado, A. Adamski, G. Adami, M. Cargnello, S. Bernal, P. Fornasiero, CuO_x-TiO_2Photocatalysts for H_2 production from ethanol and glycerol solutions, J. Phys. Chem. A 114 (2010) 3916–3925.
[16] A. Kudo, H. Kato, Photocatalytic water splitting into H_2 and O_2 over various tantalatephotocatalysts, Catal. Today 78 (2003) 561–569.
[17] M. Tian, W. Shangguoan, J. Yuan, S. Wang, Z. Ouyang, Promotion effect of nanosized Pt, RuO_2 and NiO_x loading on visible light-driven photocatalysts $K_4Ce_2M_{10}O_{30}$ (M = Ta Nb) for hydrogen evolution from water decomposition, Sci. Technol. Adv. Mater. 8 (2007) 82–88.
[18] M. Hara, T. Kondo, M. Komoda, S. Ikeda, J.N. Kondo, K. Domen, K. Shinohara, A. Tanaka, Cu_2O as a photocatalyst for overall water splitting under visible light irradiation, Chem. Commun. (1998) 357–358.
[19] H. Tian, X.L. Zhang, J. Scott, C. Ng, R. Amal, TiO_2-supported copper nanoparticles prepared via ion exchange for photocatalytic hydrogen production, J. Mater. Chem. A 2 (2014) 6432–6438.
[20] A. Heciak, A.W. Morawski, B. Grzmil, S. Mozia, Cu-modified TiO_2photocatalysts for decomposition of acetic acid with simultaneous formation of C-1-C-3 hydrocarbons and hydrogen, Appl. Catal. B:Environ. 40 (2013) 108–114.
[21] S. Linic, P. Christopher, D.B. Ingram, Plasmonic-metal nanostructures for efficient conversion of solar to chemical energy, Nature Mater. 10 (2011) 911–921.
[22] T. Sasaki, M. Watanabe, Y. Michiue, Y. Komatsu, F. Izumi, S. Takenouchi, Preparation and acid – base properties of a protonated titanate with the lepidocrocite-like layer structure, Chem. Mater. 7 (1995) 1001–1007.
[23] T.W. Kim, H. Ha, M. Paek, S. Hyun, I. Baek, J. Choy, S. Hwang, Mesoporous iron oxide-layered titanatenanohybrids: soft-chemical synthesis, characterization, and photocatalyst application, J. Phys. Chem. C 112 (2008) 14853–14862.
[24] T. Gao, H. Fjellvag, P. Norby, Defect chemistry of a zinc-doped lepidocrocitetitanate $Cs_xTi_{2-x/2}Zn_{x/2}O_4$ (x = 0.7) and its protonic form, Chem. Mater. 21 (2009) 3503–3513.
[25] H. Song, A.O. Sjastad, H. Fjellvag, H. Okamoto, O.B. Vistad, B. Arstad, P. Norby, Exfoliation and thermal transformations of Nb-substituted layered titanates, J. Solid State Chem. 184 (2011) 3135–3143.
[26] G. Liu, L. Wang, C. Sun, X. Yan, X. Wang, Z. Chen, S.C. Smith, H. Cheng, G.Q. Lu, Band-to-band visible-light photon excitation and photoactivity induced by homogeneous nitrogen doping in layered titanates, Chem. Mater. 21 (2009) 1266–1274.
[27] T. Gao, H. Fjellvag, P. Norby, Protonic titanate derived from $Cs_xTi_{2-x/2}Mg_{x/2}O_4$ (x = 0.7) with lepidocrocite-type layered structure, J. Mater. Chem. 19 (2009) 787–794.
[28] T. Sumida, Y. Takahara, R. Abe, M. Hara, J.N. Kondo, K. Domen, M. Kakihana, M. Yoshimura, Ion-exchangeable thin films derived from a layered titanate, $Cs_{0.68}Ti_{1.83}\square_{0.17}O_4$ (□:vacancy), Phys. Chem. Chem. Phys. 3 (2001) 640–644.
[29] T. Nakayama, N. Ichikuni, S. Sato, F. Nozaki, Ni/Mgo catalyst prepared using citric acid for hydrogenation of carbon dioxide, Appl. Catal. A 158 (1997) 185–199.
[30] O. Merka, D.W. Bahnemann, M. Wark, Improved photocatalytic hydrogen production by structure optimized non-stoichiometric $Y_2Ti_2O_7$, ChemCatChem 4 (2012) 1819–1827.
[31] L. Schwertmann, M. Wark, R. Marschall, Sol–gel synthesis of defect-pyrochlore structured $CsTaWO_6$ and the tribochemical influences on photocatalytic activity, RSC Adv. 3 (2013) 18908–18915.
[32] J. Soldat, R. Marschall, M. Wark, Improved overall water splitting with barium tantalate mixed oxide composites, Chem. Sci 5 (2014) 3746–3752.
[33] M. Ohashi, Preparation and lithium intercalation of layer structured titanate $Cs_xTi_{2-x/4}O_4$ (x = 0.68), Mol. Cryst. Liq. Cryst. 311 (1998) 51–56.
[34] E. Fanchon, J.L. Hodeau, J. Vicat, J.A. Watts, Three-dimensional/one-dimensional transition in the Cs^+ sublattice of the mixed valence $CsTi_8O_{16}$ hollandite: structures at 297 and 673 K, J. Solid State Chem. 92 (1991) 88–100.
[35] L.A. Bursill, J. Kwiatkowska, Location of Cs ions in a hollandite-related superstructure, J. Solid State Chem. 52 (1984) 45–52.
[36] H. Wang, F. Tam, N.K. Grady, N.J. Halas, Cu nanoshells: effects of interband transitions on the nanoparticle plasmon resonance, J. Phys. Chem. B 109 (2005) 18218–18222.
[37] T. Yamaguichi, E. Kazuma, N. Sakai, T. Tatsuma, Photoelectrochemical responses from polymer-coated plasmonic copper nanoparticles on TiO_2, Chem. Lett. 41 (2012) 1340–1342.
[38] A. Marimuthu, J. Zhang, S. Linic, Tuning selectivity in propylene epoxidation by plasmon mediated photo-switching of Cu oxidation state, Science 29 (2013) 1590–1593.
[39] M.R. Allen, A. Thibert, E.M. Sabio, N.D. Browning, D.S. Larsen, F.E. Osterloh, Evolution of physical and photocatalytic properties in the layered titanates $A_2Ti_4O_9$ (A = K, H) and in nanosheets derived by chemical exfoliation, Chem. Mater. 22 (2010) 1220–1228.
[40] H. Song, A.O. Sjastad, O.B. Vistad, T. Gao, P. Norby, Preparation of Nb-substituted titanates by a novel sol-gel assisted solid state reaction, Inorg. Chem. 48 (2009) 6952–6959.
[41] M.W. Majeski, I.L. Bolotin, L. Hanley, Appl. Mater. Interfaces 6 (2014) 12901–12908.
[42] J.F. Moulder, W.F. Stickle, P.E. Sobol, K.D. Bomben, Handbook of X-Ray Photoelectron Spectroscopy, in: J. Chastain (Ed.), Perkin Elmer Corp., Eden Prairie, MN, 1992.
[43] X-ray Photoelectron Spectroscopy Database 20, Version 3.0, National Institute of Standards and Technology, Gaithersburg, MD, 2018http://srdata.nist.gov/XPS.
[44] F.A. Cotton, G. Wilkinson, Advanced Inorganic Chemistry 4th Edition, John Wiley & Sons, 1982.
[45] N. Chandra Dutta, T. Iwasaki, T. Ebina, H. Hayashi, J. Colloid Interface Sci. 216 (1999) 161–166.